Tellus SERIES B CHEMICAL AND PHYSICAL METEOROLOGY
PUBLISHED BY THE INTERNATIONAL METEOROLOGICAL INSTITUTE IN STOCKHOLM

On the processes controlling the seasonal cycles of the air–sea fluxes of O_2 and N_2O: A modelling study

By MANFREDI MANIZZA[1]*, RALPH F. KEELING[1] and CYNTHIA D. NEVISON[2], [1]*Geosciences Research Division, Scripps Institution of Oceanography, University of California San Diego, La Jolla, CA, USA;* [2]*Institute of Arctic and Alpine Research, University of Colorado, Boulder, CO, USA*

(Manuscript received 26 March 2012; in final form 26 September 2012)

ABSTRACT

The seasonal dynamics of the air–sea gas flux of oxygen (O_2) are controlled by multiple processes occurring simultaneously. Previous studies showed how to separate the thermal component from the total O_2 flux to quantify the residual oxygen flux due to biological processes. However, this biological signal includes the effect of both net euphotic zone production (NEZP) and subsurface water ventilation. To help understand and separate these two components, we use a large-scale ocean general circulation model (OGCM), globally configured, and coupled to a biogeochemical model. The combined model implements not only the oceanic cycle of O_2 but also the cycles of nitrous oxide (N_2O), argon (Ar) and nitrogen (N_2). For this study, we apply a technique to distinguish the fluxes of O_2 driven separately by thermal forcing, NEZP, and address the role of ocean ventilation by carrying separate O_2 components in the model driven by solubility, NEZP and ventilation. Model results show that the ventilation component can be neglected in summer compared to the production and thermal components polewards but not equatorward of 30° in each hemisphere. This also implies that neglecting the role of ventilation in the subtropical areas would lead to overestimation of the component of O_2 flux due to NEZP by 20–30%. Model results also show that the ventilation components of air–sea O_2 and N_2O fluxes are strongly anti-correlated in a ratio that reflects the subsurface tracer/tracer relationships ($\sim$0.1 mmol N_2O/mol O_2) as derived from observations. The results support the use of simple scaling relationships linking together the thermally driven fluxes of Ar, N_2 and O_2. Furthermore, our study also shows that for latitudes polewards of 30° of both hemispheres, the Garcia and Keeling (2001) climatology, when compared to our model results, has a phasing error with the fluxes being too early by $\sim$2–3 weeks.

Keywords: air–sea fluxes, ocean biogeochemical cycles, ocean modeling, gas flux theory, general circulation models

1. Introduction

The surface of the oceans is the main conduit for the exchange of greenhouse and biologically active gases, such as carbon dioxide, N_2O, O_2 and dimethyl sulphide between air and the ocean interior. The gas for which we have the most observational information and which is central to ocean biogeochemistry is O_2 (Najjar and Keeling, 1997). A starting point to understand how the air–sea exchange of this gas could respond to climate change (Bopp et al., 2002; Keeling and Garcia, 2002; Matear and Hirst, 2003; Shaffer et al., 2009) is to elucidate on the controls the response to the changes in physical forcing associated with the seasons (Najjar and Keeling, 2000).

For instance, the seasonal exchange of O_2 between the atmosphere and ocean provides important insights into a range of physical and biogeochemical processes. At middle and high latitudes, O_2 tends to be released to the atmosphere by net photosynthesis in summer, while O_2 tends to be taken up in winter as O_2-depleted subsurface waters are ventilated during deep mixing processes (Riser and Johnson, 2008). Together with these biologically driven exchanges are additional exchanges driven by solubility changes, which also cause O_2 to be outgassed in summer and ingassed in winter as the waters warm and cool (Najjar and Keeling, 2000). Measurements of O_2 in surface waters, often combined with additional data [for instance, dissolved inorganic carbon as showed by Bates et al. (2005)],

*Corresponding author.
email: mmanizza@ucsd.edu

Citation: Tellus B 2012, **64**, 18429, http://dx.doi.org/10.3402/tellusb.v64i0.18429

have provided estimates of the rates of net community production (NCP) in surface waters, a fundamental measure of carbon uptake that is closely tied to the export of organic matter into the ocean interior (Brix et al., 2006). The seasonal cycling of O_2 between the ocean and the atmosphere also leads to detectable changes in the atmospheric O_2/N_2 ratio, which have also been exploited to constrain rates of production in the ocean (Keeling and Shertz, 1992).

Deriving estimates of NCP from dissolved O_2 measurements require correcting the impact of solubility changes and ventilation processes to isolate the changes due to photosynthesis. Early studies typically assumed that the solubility-driven changes were simply tied to solubility itself, such that the biological influences are tied to the degree of super- or under-saturation with respect to the atmosphere (Shulenberger and Reid, 1981), or equivalently tied to the apparent oxygen utilisation (AOU). An essentially equivalent assumption, applied to the interpretation of atmospheric O_2/N_2 data, has been that the seasonal exchange of O_2 driven by solubility is simply tied to the net air–sea heat flux (Keeling et al., 1993). A more refined approach to the interpretation of dissolved O_2 data is to use concurrent measurements of dissolved Ar (Craig and Hayward, 1987), an inert gas with nearly the same solubility as O_2. Dissolved Ar provides a measure of how O_2 would behave without biological influences, including disequilibria driven by solubility changes. A parallel approach to the interpretation of atmospheric O_2/N_2 data would be to estimate the solubility component of the O_2/N_2 changes using concurrent measurements of seasonal changes Ar/N_2 ratio.

These approaches, however, only address the thermal component of the air–sea O_2 flux. Additional assumptions are needed to further separate the ventilation and production components. These changes can also directly impact the abundance of O_2 in subsurface waters, which is crucial for the oceanic environment not only for supporting marine life (Keeling et al., 2010) but also because it can influence the subsurface production of N_2O.

One approach is to restrict attention to the spring and summer, when the water column is strongly stratified and rates of photosynthesis are high. At this time of year, it may be reasonable to assume that the ventilation component can be neglected altogether, an approach adopted in various studies (Najjar and Keeling, 2000; Hendricks et al., 2004; Stanley et al., 2010). The production component is then viewed as the difference between the total air–sea O_2 flux and the thermal component for this time of year. One of our goals is to examine the range of validity of this assumption.

Another approach to separating ventilation and production components is to exploit linkages between the ventilation fluxes of O_2 and the flux of N_2O. Field studies have shown a strong correlation between oxygen defect at subsurface due to respiration and N_2O excesses due to N_2O production (Yoshinari, 1976; Butler et al., 1989; Nevison et al., 2003; Walter et al., 2006). The formation of N_2O in the ocean occurs through the process of nitrification, in which ammonium (NH_4^+) is oxidised to nitrate (NO_3^-), via an aerobic two-step processes of which N_2O is a by-product (Beman et al., 2011). N_2O is also produced via denitrification or coupled nitrification–denitrification in zones of the ocean where the concentration of O_2 is highly depleted (Naqvi et al., 1998, 2009). In these regions, NO_3^- becomes a preferential electron acceptor in place of O_2, and N_2O is formed as an obligate intermediate of denitrification. N_2O production via both nitrification and denitrification occurs predominantly in the subsurface ocean. The subsurface water masses of the world oceans are thus not only typically undersaturated in O_2 but also supersaturated in N_2O.

Measurements have shown the tight coupling between O_2 and N_2O both in the subsurface (where water masses are vertically placed) and in the lower atmosphere where these waters upwell, that is, the coastal upwelling system along the coast of Oregon and California (Lueker et al., 2003) and in the Northern Pacific Ocean (Dore et al., 1998). Nevison et al. (2005), based on this empirical evidence, used atmospheric observations of N_2O to estimate the biological air–sea N_2O flux and the corresponding air–sea O_2 flux due to subsurface ventilation in the Southern Ocean where the upwelling of deep waters is a permanent oceanographic feature due to the constant action of the westerly winds over the ocean surface. Subsurface water masses, when ventilated by circulation to the ocean surface, carry with them that specific biogeochemical signature that can be also detected in the air overlaying that portion of ocean surface (Lueker et al., 2003) where upwelling occurs (Law and Owens, 1990) and where transported by air mixing. Here, we explore the validity of this approach in the context of an ocean general circulation model (OGCM) simulation that couples O_2 and N_2O fluxes.

The optimal method for computing the thermal component of the O_2 fluxes is a matter for on-going discussion. To compute the O_2 thermal flux Keeling and Shertz (1992) proposed simple scaling formula based on the solubility temperature derivative and on the air–sea heat fluxes. Later, Jin et al. (2007) also refined the estimation of the thermally driven O_2 flux proposed by Keeling and Shertz (1992) to better match the phase and the amplitude of the same fluxes computed by an OGCM. They showed that the parameterisation proposed by Keeling and Shertz (1992) could not fully explain the thermal O_2 flux explicitly computed by their model, an OGCM that explicitly takes into account the mixed layer physics and its effects on air–sea gas exchange. Compared to their model, the Keeling

and Shertz (1992) method overpredicts the thermally driven flux by 30%. Instead, they proposed a modified formula in which the Keeling and Shertz (1992) fluxes are scaled downwards by a fixed factor (1/1.3) and delayed by 2 weeks. However, the study of Jin et al. (2007) leaves open several key questions. First, whether the results with their approximation can be successfully applied to other ocean models to generate a good agreement between diagnostic and prognostic fluxes. Second, if such approximation can be applied to other gases such as nitrogen and argon that have only thermally driven flux component.

Several studies based on observations (Garcia and Keeling, 2001; Keeling and Garcia, 2002) showed that a robust correlation exists, not just between heat and the thermal component of the O_2 flux but also between heat and the total O_2 flux. This implies that the biological component of the total O_2 flux as well as the thermal component is also closely tied to the flux of heat. However, this important aspect has never been explored in the mechanistic context of an OGCM.

Here, we use a large-scale OGCM to explore several unresolved questions involving the air–sea exchange of O_2 in relation to fluxes of heat and fluxes of N_2O, N_2 and Ar. The OGCM includes a biogeochemical module that explicitly represents the full cycles of O_2 and N_2O and the oceanic cycles of N_2 and Ar and further separates the cycles of O_2 and N_2O into different components driven by different processes, including photosynthesis, ventilation and thermal effects. We will use this model to address the following questions:

(1) What is the role of ocean ventilation in the seasonal cycle of O_2 at different latitudes and to what extent can we assume that the role of ocean ventilation is negligible when estimating the summertime air–sea O_2 flux due to NCP as proposed by Najjar and Keeling (2000)?
(2) How well does the ventilation N_2O flux correlate with the O_2 ventilation flux?
(3) How well does the relation for the thermal fluxes proposed by Jin et al. (2007) work in this model?
(4) What is the relationship between the O_2, N_2 and Ar thermally driven fluxes and does a simple solubility scaling suffice for computing one from the other?
(5) What is the relationship between total O_2 air–sea gas flux and the air–sea heat flux in this model when compared to the Garcia and Keeling (2001) climatology?

This article is organised in the following way: In Section 2, we describe the ocean physical–biogeochemical model used and the cycles of various tracers implemented and discussed in this study. In Section 3, we show the results obtained from which we both evaluate our model and discuss the findings emerging from our study. In Section 4, we summarise the main results and suggest potential future research directions.

2. Methods

2.1. Ocean physical–biogeochemical model

We use the MIT general circulation model (MITgcm) (Marshall et al., 1997) with a coarse resolution configuration (2.8° by 2.8°) and 15 vertical levels whose first two uppermost boxes are 50 and 70 m thick, respectively. The time step is 900 seconds for ocean physics and 43 200 seconds for the biogeochemical tracers. The physical set-up has a closed northern boundary at 80°N so that the Arctic Ocean is not fully represented. The effects of unresolved mesoscale eddy mixing is parametrised according to Gent and McWilliams (1990) with isopycnal mixing coefficients of $1 \times 10^3\ m^2\ s^{-1}$. The OGCM is forced with climatological annual cycles of wind speed from Trenberth et al. (1989) and heat and freshwater fluxes are applied according to Jian et al. (1999). We apply to the model a seasonal sea–ice cover following the approach adopted by Dutkiewicz et al. (2005) that is repeated for each simulated year.

In the OGCM, we embed an ocean biogeochemical model that explicitly represents the dynamics of the pelagic ecosystem. The biogeochemical model has been developed by Dutkiewicz et al. (2005) and is used for biogeochemical applications (Ito et al., 2005). The original biogeochemical model developed by Dutkiewicz et al. (2005) includes two phytoplankton functional types (diatoms and non-diatoms) and one generic zooplankton functional type and carries 19 biogeochemical tracers. The biological production is limited by the availability of light and nutrients (phosphorus, silicon and iron). In regions where sea–ice is present, the surface incoming solar radiation is reduced according to the sea–ice cover fraction imposed to the model. As shown by Dutkiewicz et al. (2005), the physical–biogeochemical model used for this study gives a fairly realistic representation of the three-dimensional distribution of the macro nutrients (phosphate and silicate) and captures the main patterns of surface distribution of chlorophyll concentration with low values in the subtropical gyres and high values at high latitudes and at the equator. Further details in the biogeochemical model can be found in Dutkiewicz et al. (2005). The model also represents a full cycle of O_2 that interacts with the pelagic ecosystem dynamics so that the processes of primary production carried out by the phytoplankton groups and heterotrophic respiration impact the O_2 concentration (Bennington et al., 2009).

For this study, we add new tracers, such as N_2, Ar and N_2O, to the original biogeochemical model. We also add

two specific tracers that selectively represent several processes affecting the biogeochemical cycling of O_2, as will be discussed below in the Section 2.2.

2.2 Modelling and decomposition of air–sea gas fluxes

The time evolution of each generic biogeochemical tracer C is governed by the following generic expression:

$$\frac{\partial C}{\partial t} = T_C + \mathrm{SMS} \tag{1}$$

$$T_C = -u \cdot \nabla C + \nabla \cdot (K \nabla C) \tag{2}$$

where the first $T_{(C)}$ represents altogether the three-dimensional tracer advection and diffusion due to ocean physical processes, respectively, whereas SMS stands for 'sources minus sinks' that includes all the biogeochemical processes regulating the concentration of any tracer C. For O_2, the generic equation shown above expands as follows:

$$\frac{\partial O_2}{\partial t} = T_{O_2} + \mathrm{SMS} \ \text{ where } \ \mathrm{SMS} = \mathrm{NCP} \tag{3}$$

where $\mathrm{NCP} = \mathrm{PP} - \mathrm{R}$; PP stands for primary production and R for respiration and are calculated by the ocean ecosystem model (Dutkiewicz et al., 2005).

To separate the air–sea O_2 fluxes into components due to thermal, NCP and ventilation effects, we also introduce the tracers 'Thermal Oxygen' ($O_{2(\mathrm{Th})}$) and 'Aphotic Oxygen' ($O_{2(\mathrm{Ap})}$). The $O_{2(\mathrm{Th})}$tracer is influenced only by the heat fluxes at the ocean surface that, varying seasonally, determines the solubility of O_2 in seawater, as indicated below:

$$\frac{\partial O_{2(\mathrm{Th})}}{\partial t} = T_{O_{2(\mathrm{Th})}} + \mathrm{SMS} \ \text{ where } \ \mathrm{SMS} = 0 \tag{4}$$

The equation governing the temporal evolution of 'Aphotic Oxygen' ($O_{2(\mathrm{Ap})}$) is the same as for O_2 with the only difference being setting the terms of PP and R to zero, if and only if when their difference (therefore NCP) is positive, as follows:

$$\frac{\partial O_{2(\mathrm{Ap})}}{\partial t} = T_{O_{2(\mathrm{Ap})}} + \mathrm{SMS} \tag{5}$$

$$\text{where } \mathrm{SMS} = 0 \quad \text{if} \ \ \mathrm{NCP} \geq 0 \tag{6}$$

$$\text{or } \mathrm{SMS} = \mathrm{NCP} \quad \text{if} \ \ \mathrm{NCP} < 0 \tag{7}$$

$O_{2(\mathrm{Ap})}$ is effectively the O_2 concentration that is obtained from the combined influences of gas exchange, thermal solubility influences and consumption of O_2 below the euphotic zone, which is defined dynamically based on the $\mathrm{NCP} > 0$ criterion. For both $O_{2(\mathrm{Th})}$ and $O_{2(\mathrm{Ap})}$, the model computes the corresponding air–sea gas flux (F), as described below.

By subtracting the flux of $O_{2(\mathrm{Ap})}$ from the total flux of O_2, we can isolate the flux due to process of production of organic matter ($O_{2(\mathrm{Prod})}$):

$$O_{2(\mathrm{Prod})} = O_2 - O_{2(\mathrm{Ap})} \tag{8}$$

Similarly, we can isolate the O_2 flux component due to the physical process of ocean ventilation ($O_{2(\mathrm{Vent})}$):

$$O_{2(\mathrm{Vent})} = O_{2(\mathrm{Ap})} - O_{2(\mathrm{Th})} \tag{9}$$

The subtraction in Eq. (8) cancels both the solubility and aphotic respiratory contributions to the O_2 concentration, leaving only the contribution from NCP in the euphotic zone. The subtraction in Eq. (9) similarly cancels the solubility component, leaving the component due to respiration in the aphotic zone, which we refer to as the ventilation component. The total O_2 content can thus be divided into three components: (1) thermal; (2) production; and (3) ventilation as follows:

$$O_{2_{(\mathrm{Tot})}} = O_{2_{(\mathrm{Th})}} + O_{2_{(\mathrm{Prod})}} + O_{2_{(\mathrm{Vent})}} \tag{10}$$

The air–sea fluxes fluxes can be similarly divided in three components:

$$F_{(\mathrm{Tot})} = F_{(\mathrm{Th})} + F_{(\mathrm{Prod})} + F_{(\mathrm{Vent})} \tag{11}$$

$$F_{(\mathrm{Prod})} = F_{(\mathrm{Tot})} - F_{(\mathrm{Ap})} \tag{12}$$

$$F_{(\mathrm{Vent})} = F_{(\mathrm{Ap})} - F_{(\mathrm{Th})} \tag{13}$$

The equation governing the time–evolution of N_2O has two terms:

$$\frac{\partial N_2O}{\partial t} = T_{N_2O} + \mathrm{SMS} \tag{14}$$

$$\mathrm{SMS} = J_{N_2O} \tag{15}$$

where the first term represents the contribution due to ocean physics and the second term J_{N2O} (corresponding to the SMS generic term) represents the production or consumption of N_2O in the water column (that depends on the production and consumption of O_2). To parameterise the term J_{N2O}, we implemented the same model developed by Suntharalingam and Sarmiento (2000) who proposed to parameterise it in the following way:

$$J_{N_2O} = A_o \, e^{\frac{z - z_{eu}}{z^*}} \cdot R \tag{16}$$

where A_o is 0.1211×10^{-3} (mol N_2O)/(mol AOU), z is the depth, z_{eu} is the depth of the euphotic zone (fixed at 100 m for this study), z^* is 3333 m and R stands for respiration computed by the model at each vertical level. This parameterisation, based on oceanic observations of O_2 and N_2O, allows for N_2O production, where O_2 respiration is greater than O_2 production (mostly in the subsurface layers of the ocean). The value of A_o represents the mean

ratio that links the rate of AOU and the consequent production rate of N_2O. As proposed by Suntharalingam and Sarmiento (2000), we also shut off the production of N_2O in the first two uppermost boxes of the model to indirectly represent the effect of light inhibition on denitrification (Horrigan et al., 1981). As we did for O_2, we add another tracer for N_2O that has no biogeochemical sources or sinks but that has the same solubility properties as N_2O air–gas exchange flux and we define it as N_2O-Thermal ($N_2O_{(Th)}$), as shown below:

$$\frac{\partial N_2O_{(Th)}}{\partial t} = T_{N_2O_{(Th)}} + SMS \tag{17}$$

$$SMS = 0 \tag{18}$$

With the use of these two tracers, we can derive then a third indirect tracer called $N_2O_{(Vent)}$ that give us information on the distribution and the fluxes of N_2O only driven by ocean ventilation, as indicated below:

$$N_2O_{(Vent)} = N_2O - N_2O_{(Th)} \tag{19}$$

As already shown in the case of O_2, the same concept of separation of the tracers can be applied to the air–sea gas fluxes of N_2O, as follows:

$$F_{(Vent)} = F_{(Tot)} - F_{2(Th)} \tag{20}$$

For this study, we also implement in our OGCM the cycle of two inert gases, Ar and N_2. Their cycle is described by Eq. (1) where the SMS term is equal to zero for both gases as done for thermal components of O_2 and N_2O. The air–sea exchange of each gas described above and discussed in this study is prognostically computed by the ocean biogeochemical model and parametrised in the following way:

$$Flux_{(air-sea)} = K_w\ (C - C_{eq})\ (1 - \gamma) \tag{21}$$

where K_w is the gas-transfer velocity that depends primarily on the wind speed (Wanninkhof, 1992), C is the gas concentration at ocean surface, C_{eq} is the concentration in equilibrium with the atmosphere and g is the sea–ice cover fraction that varies seasonally (ranging between 0 and 1) in the polar oceans. The gradient driving the air–gas flux ($C - C_{eq}$) is computed calculating the departure of surface concentration (C) from the saturation value (C_{eq}) from temperature and salinity computed *on-line* by the OGCM. K_w is computed according to the following formula:

$$K_w = 0.31 \cdot u^2 \cdot (Sc/660)^{-1/2} \tag{22}$$

when u is the wind speed and Sc indicates the Schmidt number that depends on seawater temperature according to specific coefficients that vary from gas to gas as also reported by Wanninkhof (1992). The solubility coefficients for Ar and N_2 are taken from Hamme and Emerson (2004) while those for O_2 and N_2O are from Garcia and Gordon (1992) and Weiss and Price (1980), respectively. Air–sea fluxes of $O_{2(Th)}$, $O_{2(Ap)}$ and $N_2O_{(Th)}$ are computed using saturation values of O_2 and N_2O, respectively. For this study, we run our biogeochemical model for 2000 yr and we analyse the output of the last year generating a monthly output to resolve the seasonal cycle of the year.

3. Results and discussion

3.1 Biogeochemical model evaluation

We first show how the ocean biogeochemical model reproduces some key biogeochemical features of the global ocean that are important for this study. For comparison purposes, we use the same diagnostic used by Garcia and Keeling (2001), that is, the seasonal outgassing anomaly (SOA) of O_2 air–sea flux as also directly shown in our study (Fig. 1, right panels). The SOA of O_2 is computed by subtracting from each monthly value the annual mean in each model grid point. In our model, the SOA of O_2 fluxes for June and December (Fig. 1, left panels) show that the high latitudes are the regions of the oceans with the largest SOA values showing O_2 ingassing in winter and O_2 outgassing in summer of each hemisphere, due to the solubility and biological effects working in synergy in each month. Our results are in fair agreement with the results shown by Garcia and Keeling (2001) (Fig. 1, right panels) because they match fairly well with their spatial patterns and they show a comparable magnitude for the air–sea gas flux.

To evaluate the model depiction of N_2O, we compare the spatial distribution computed by our biogeochemical model in the three main ocean basins (Fig. 2) against observations (Nevison et al., 2003; Walter et al., 2006). The data from Nevison et al. (2003) are directly shown in this study to evaluate our model results.

In the Atlantic basin (Fig. 2), the model captures the high values of [N_2O] in the tropical zone at subsurface and the low values (10 nM) in the extra tropical zones in the top 500 m of the water column. The vertical distribution of [N_2O] in the North Atlantic is also comparable to the data shown by Walter et al. (2006) in the same basin from the tropics to the subpolar regions, with a subsurface maximum that increases in concentration from the high latitude to the tropical oceans where our model overestimates the value of the subsurface peak (50 nM) when compared to their study (30 nM).

In the Pacific Ocean, the biogeochemical model reproduces the general features of the vertical distribution of the [N_2O] (Fig. 2) in the top 1500 m of the ocean when

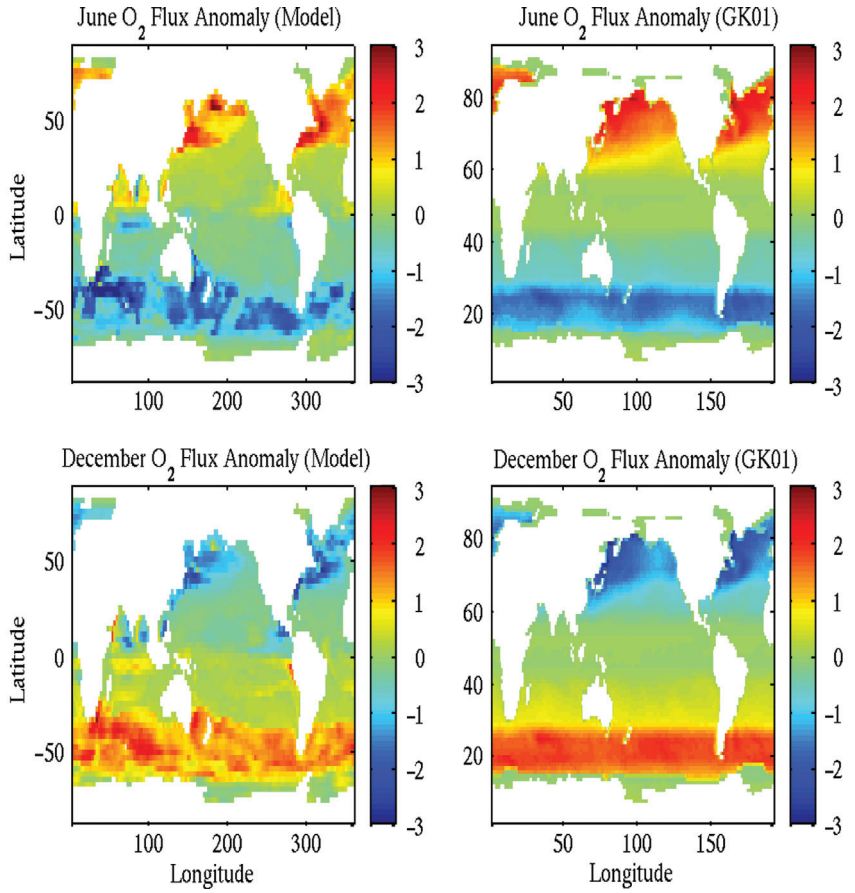

Fig. 1. Seasonal anomaly of air–sea O_2 flux for (top) June and (bottom) December computed by (left) our ocean biogeochemical model and (right) from the fluxes of Garcia and Keeling (2000). Positive values correspond to outgassing.

compared to available observations (Fig. 3) taken form the study of Nevison et al. (2003).

In the Indian Ocean, the biogeochemical model reproduces fairly realistically the distinct observed gradients of [N_2O] between the northern and the southern part of the oceanic basin (Fig. 2, bottom panel) as shown by the vertical profiles of [N_2O] shown by Nevison et al. (2003) (Fig. 3). In the top 1500 m of the water column, the northern Indian Ocean is characterised by the high values of [N_2O] (50–80 nM) due to the reduced ventilation and high utilisation of dissolved oxygen observed in this area. Lower values of [N_2O] (10–20 nM) are found in the southern part of the Indian Ocean.

The model results of air–sea fluxes show that the western boundary currents of the northern oceans, the Southern Ocean, the northern sector of the Indian Ocean and the Equatorial Pacific Ocean are the main regions of N_2O outgassing (Fig. 4). The air–sea N_2O flux occurs in the Southern Ocean due to wind-driven upwelling (Fig. 4) that brings to the surface water coming from deeper layers of that oceanic region, where O_2 is undersaturated and N_2O is supersaturated (Nevison et al., 2003, 2005, 2012).

Our results are also are in fair agreement with those obtained by Suntharalingam and Sarmiento (2000) who developed and implemented the parameterisation that we adopted for this study. Our results are also comparable with the estimates provided by Nevison et al. (1995) based on oceanic observations. Our model also produces a global annual outgassing equal to 4.5 TgN yr^{-1} comparable to estimates currently available: 1.2–6.8 TgN yr^{-1} (Nevison et al., 1995), 3.8 TgN yr^{-1} (Suntharalingam and Sarmiento, 2000) and 5.8 ± 2 TgN yr^{-1} (Nevison et al., 2003). However, the discrepancies between our model results and the previous estimates of air–sea fluxes of N_2O are not discussed in detail because they are not the primary goal of this study.

Our model also computes a global annual average of NCP equal to $\sim$11 P gC yr^{-1} ($P = 10^{15}$) when integrated into the top 120 m of the water column that is comparable to the estimates of carbon export production reported by Schlitzer (2000).

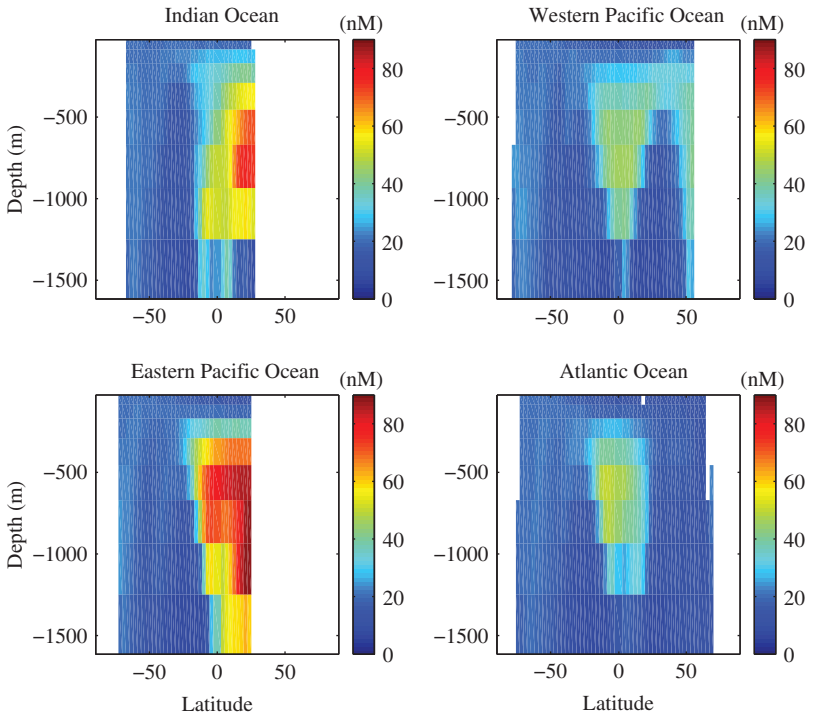

Fig. 2. Vertical sections of $[N_2O]$ in four locations of the global ocean as computed by the ocean biogeochemical model. Values refer to annual mean and units are nM.

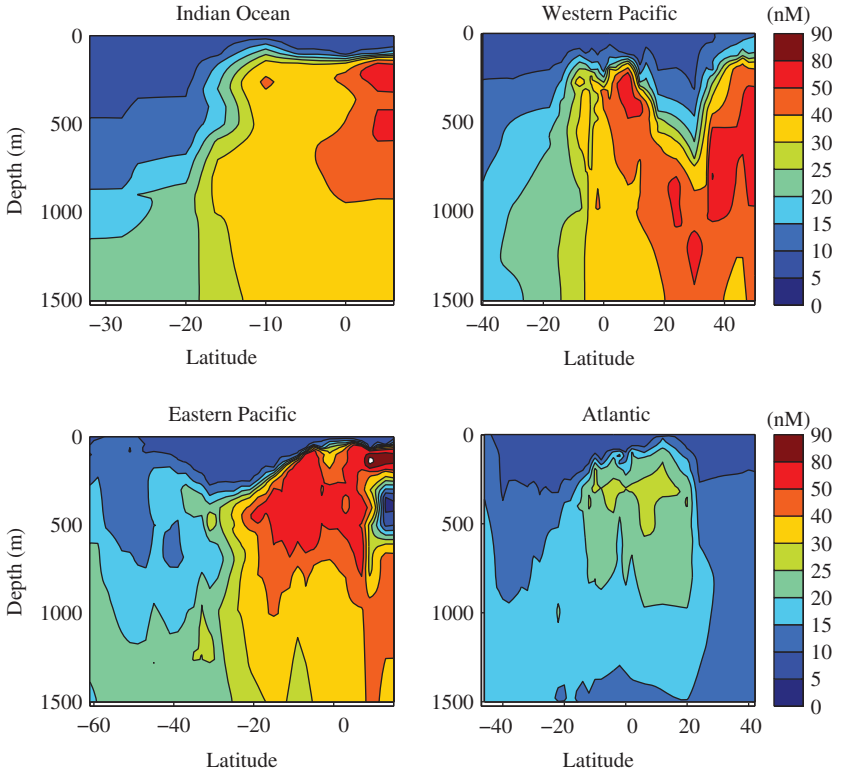

Fig. 3. Vertical sections of observed $[N_2O]$ in four locations of the global ocean. Units are nM.

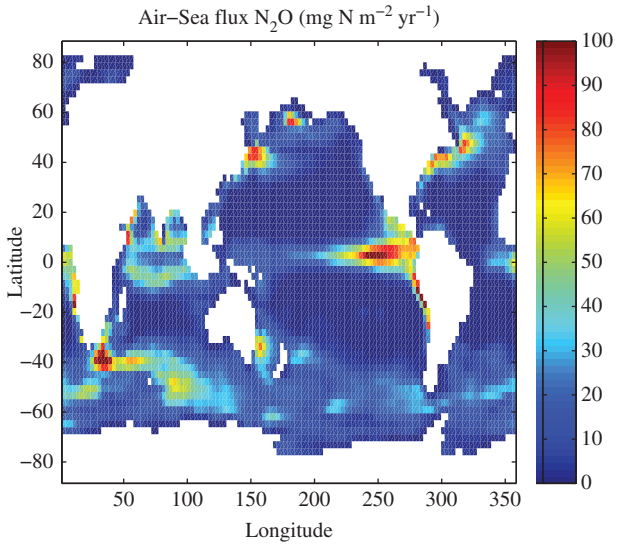

Fig. 4. Annual mean of air–sea fluxes of total N_2O computed by the ocean biogeochemical model. Units are mg N $m^{-2}yr^{-1}$.

3.2. *Seasonal decomposition of air–sea gas fluxes*

For the purpose of presenting the seasonal cycle of the gas fluxes, we divide the global ocean into five sectors that are then zonally averaged: the tropics (10°N–10°S), the mid-latitudes (10°–30°) and the high-latitudes (>30°) of each hemisphere.

The top panels of Figs. 5, 6 and 7 also show the net euphotic zone production (NEZP) of O_2 (Keeling and Shertz, 1992) defined as the vertical integral of NCP over the euphotic zone, that is, the depth range where NCP is greater than zero. NEZP is a measure of production per unit ocean surface area. In practice, we consider contributions to the NEZP integration only down to 120 m (the first two top model layers) as NCP is uniformly negative below that depth. We report NEZP in units of O_2 production, which is related in our model to carbon production via the constant Redfield ratio of 1.4, as shown by the green lines of the top panels in Figs. 5, 6 and 7. The integration accounts exactly for the sources that drive the $O_{2(Prod)}$ tracer, so that NEZP can be closely related to the flux due to production, $F_{(Prod)}$. In a limiting (idealised) case where euphotic zones equilibrated instantaneously with the overlying air, NEZP and $F_{(Prod)}$ would be identical because the O_2 produced would be instantaneously outgassed. As shown in the top panels of Figs. 5, 6 and 7, the seasonal cycle in $F_{(Prod)}$ is damped and lagged compared to the cycle in NEZP. This is, as expected, due to the finite gas exchange rates and because some of the euphotic zones sometimes extending below the mixed layer.

The tropical regions are characterised by steady winds that cause upwelling of waters rich in nutrients but poor in O_2 leading to fairly continuous outgassing for the production component ($F_{(Prod)}$) and ingassing for the ventilation component ($F_{(Vent)}$), as shown in Fig. 5. The $F_{(Prod)}$ and $F_{(Vent)}$ are comparable in magnitude, largely offsetting each other in the net flux. Similar to Jin et al. (2007), we find that the thermal component of the O_2 flux ($F_{(Therm)}$) has two maxima, in March and October, which follow the pattern of heat flux of the tropical regions. The total air–sea flux of N_2O (blue full line) in the tropical regions is dominated by the effect of ocean ventilation (magenta dashed line) linked to the wind-driven upwelling (Fig. 5).

In the mid-latitudes of both hemispheres, the decomposition of the air–sea O_2 fluxes (Fig. 6) shows that in the warming seasons (spring–summer), the $F_{(Prod)}$ (green full line) and $F_{(Therm)}$ (red full line) work in synergy to drive the flux of O_2 out of the ocean. Conversely, the cooling seasons' (fall–winter) ventilation (magenta dashed line) and water cooling (red line) drive the O_2 flux into the ocean, as shown by their corresponding fluxes, $F_{(Therm)}$ and $F_{(Vent)}$, respectively. In the mid-latitudes, the ventilation components of O_2 and N_2O (magenta dashed lines) are anti-correlated in their respective seasonal cycles, as also suggested by Lueker et al. (2003). As seen in Fig. 6 (top panel), the seasonal cycle of $F_{(Prod)}$ is very similar to the cycle of NEZP, but in detail is slightly lagged and has smaller magnitude. This difference is, as expected, due to finite gas exchange rates and due to the euphotic zones sometimes being deeper than the mixed layer.

In the high-latitude zones, the air–sea O_2 flux reveals (Fig. 7) differences from those highlighted for the air–sea O_2 fluxes in the mid-latitudes. The air–sea flux of O_2 due to ventilation ($F_{(Vent)}$, magenta dashed line, Fig. 7) reduces dramatically during the summer showing a remarkable difference with the same component during fall–winter when it dominates the total air–sea O_2 fluxes of the same period. This is due to the seasonal breakdown of vertical stratification of the water column. During the spring–summer months of both hemispheres, the total air–sea O_2 flux is dominated by the combination of the $F_{(Therm)}$ and $F_{(Prod)}$ whereas the $F_{(Vent)}$ goes to minimum value corresponding to 2 mol $m^{-2}yr^{-1}$ (magenta dashed line, Fig. 7) due to the seasonal vertical stratification. In the high-latitude oceans, the total air–sea fluxes of N_2O (blue line) are mostly dominated by the process of ocean ventilation (magenta dashed line) in both hemispheres (Fig. 7). As in the mid-latitudes, $F_{(Prod)}$ is very similar to NEZP itself, with only a modest lag and amplitude reduction.

The contrasting behaviour of the O_2 ventilation component between middle and high latitudes is most likely

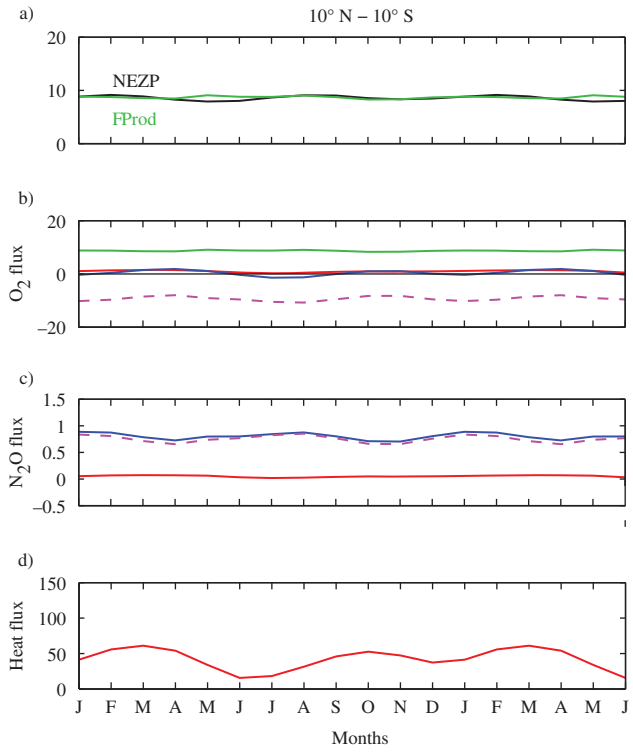

Fig. 5. Global zonal average of the seasonal cycle of modelled quantities. Panel a compares the flux due to the production ($F_{(Prod)}$, green line) with the net euphotic zone production (NEZP, black line); panel b shows single components of the air–sea O_2 flux; panel c shows air–sea N_2O flux; and panel d shows heat flux for the latitudinal band between 10°N and 10°S as zonal average. In panels b and c, the full blue line indicates the total flux, the full red line the thermal component, the dashed magenta line the ventilation component and the full green line the production component. The first 6 months are repeated to show one and a half annual cycles. Positive values indicate both outgassing and ocean heat gain. Units are mol m^{-2} yr^{-1} for air–sea gas fluxes, and W m^{-2} for heat fluxes.

explained by differences in the water column structure between these two regions. In the high latitudes, the stratification is highly seasonal, with very little vertical mixing in the summer and a vertical [O_2] gradient that has been weakened by the presence of strong ventilation the previous winter. However, in the subtropical band, the vertical mixing is much less seasonal and as a result there is a stronger vertical gradient in [O_2] which drives a ventilation flux year round. Some of the ventilation-driven O_2 flux in the subtropical regions could also be influenced by the O_2-poor tropical subsurface waters, which is then laterally advected away from the tropics to the subtropics.

This difference between the middle- and the high-latitude regions has important implications for the method of subtracting the thermally driven air–sea O_2 flux from the total air–sea O_2 flux to infer the productivity-driven flux, as adopted by Najjar and Keeling (2000). Our model results would suggest that during the warm season of each hemisphere, the ventilation component in the high-latitude oceans accounts for $\sim$10% of the total O_2 air–sea flux, whereas in the mid-latitude ocean this component driven by ocean circulation can be up to 40% of the total O_2 flux. Our results support the methods of computing summertime productivity based on mixed-layer O_2 budget (Najjar and Keeling, 2000; Hendricks et al., 2004; Stanley et al., 2010) when applied poleward but not equatorward of 30° latitude.

It is also evident from Fig. 8 that during the months of high levels of stratification (spring–summer) in the high latitudes, the ratio between the ventilation component over the production component of O_2 fluxes reaches it minimum values while in the tropical and subtropical regions such drastic seasonal variations is not evident. This is valid both for the global ocean and each single oceanic basin.

The separation between the Atlantic and the Pacific Ocean basins also highlights that the ratio in the northern high-latitude systems is directly influenced by the different strength of winter convection (and hence ventilation). This in turn is reflected by the ratio between the ventilation and production components of the air–sea O_2 fluxes. In the subpolar North Atlantic Ocean (Fig. 8, upper right panel), the ratio between the components of O_2 fluxes varies more dramatically with the season when compared to the subpolar North Pacific Ocean (Fig. 8, lower left panel).

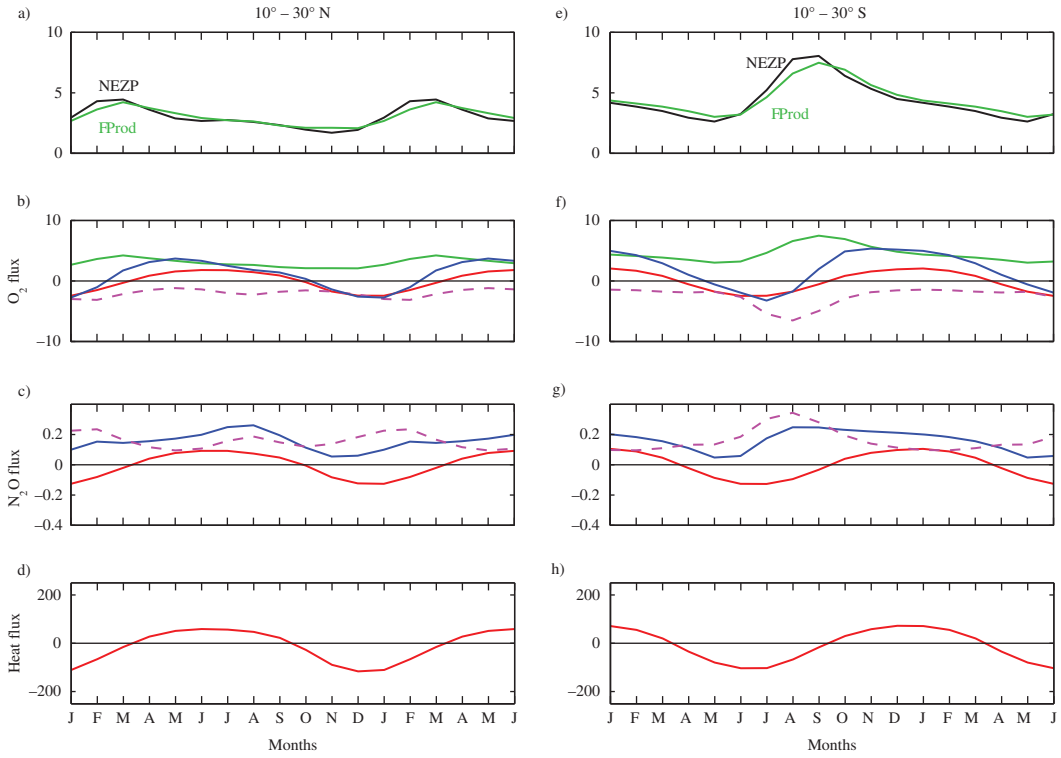

Fig. 6. Global zonal average of the seasonal cycle of modelled quantities. Panels a and e compare the flux due to the production ($F_{(\mathrm{Prod})}$, green line) with the net euphotic zone production (NEZP, black line); panels b and f show single components of the air–sea O_2 flux; panels c and g show air–sea N_2O flux; and panels d and h show heat flux for the latitudinal band between 10° and 30° of each hemisphere as zonal average. In panels b, c, g and f, the full blue line indicates the total flux, the full red line the thermal component, the dashed magenta line the ventilation component and the full green line the production component. The first 6 months are repeated to show one and a half annual cycles. Positive values indicate both outgassing and ocean heat gain. Units are mol m^{-2} yr^{-1} for air–sea gas fluxes and W m^{-2} for heat fluxes.

This difference is due to the fact that in the subpolar North Atlantic Ocean, winter convection is stronger than in the subpolar North Pacific Ocean (Warren, 1983; Weaver et al., 1999).

3.3. *Air–sea O_2 and N_2O ventilation fluxes*

The decomposition of the fluxes also allows us to test the hypothesis of the anti-correlation of the ventilation flux of O_2 and N_2O as inferred from the observations (Lueker et al., 2003). The hypothesised anti-correlation depends on the fact that N_2O is produced in zones where O_2 is consumed, as also mathematically represented in the parameterisation used in our study. As a consequence, we expect that in our model the upwelling of the same water masses would cause both an outflux of N_2O and an influx of O_2. We examined this effect in the same five latitudinal ranges used for the air–sea O_2 fluxes in the previous section. In all five regions we considered, the components of air–sea fluxes of N_2O and O_2 due to ocean ventilation only are strongly anti-correlated (Fig. 9) although the correlation varies slightly depending on the oceanic regions. It is interesting to note that the linear fit to the flux scatter plots (Table 1) approximately corresponds to the value of A_o ($\sim 0.12 \cdot 10^{-3}$) set in our biogeochemical parameterisation that takes into account the values of $\Delta N_2O/AOU$ derived from oceanic observations (Suntharalingam and Sarmiento, 2000). This is also due to the fact that the exponential term used in the parameterisation used for this study is equal to ~ 1 so that the dominant term that determines the relationship between O_2 and N_2O in the ocean interior is A_o which is also reflected in the ventilation-driven fluxes. This value is also consistent with the value reported by Lueker et al. (2003) for the northern Californian coast influenced by the California Current system. In our model, the ventilation flux ratios in the California Current, Humboldt Current and Canary Upwelling system are $0.16 \cdot 10^{-3}$, $0.13 \cdot 10^{-3}$ and $0.15 \cdot 10^{-3}$, respectively. All of these values are similar to A_o.

In our first attempt, the model of N_2O production that we used is certainly highly simplified and less comprehensive than other models (Suntharalingam et al., 2000, 2012) which represent more extensively all the processes controlling the N_2O abundance in the ocean.

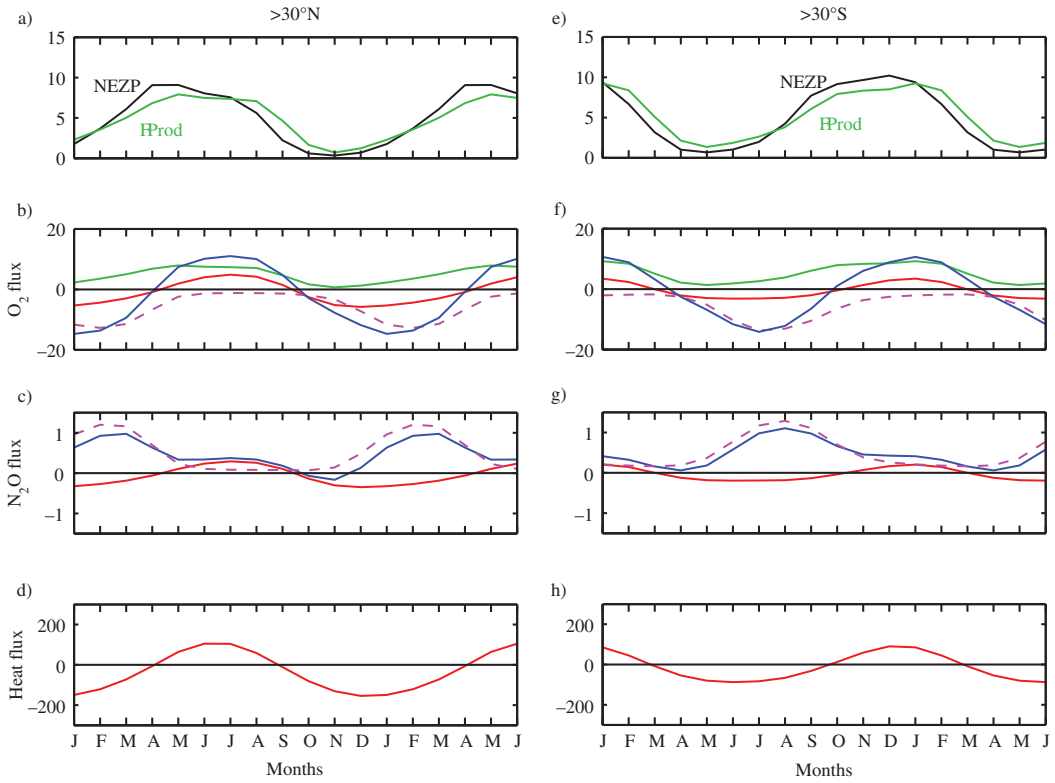

Fig. 7. Same as previous figure but for high latitude bands ($>30^{\circ}$) of each hemisphere.

Nevertheless, we verified in our model that the ratio of $\Delta N_2O/AOU$ in the subsurface layers is roughly equivalent to 0.1 mmol/mol, matching values observed in the real ocean (and also used to build our parameterisation) as reported in Table 1. This confirms the close relationship between N_2O production and O_2 consumption. Furthermore, the recent findings of Nevison et al. (2012), using the same model results presented here, confirmed that the typical signature of the ratio between N_2O production and O_2 consumption taking place in certain water masses can propagate not only to the corresponding fluxes (driven by ventilation only) but also up to the corresponding atmospheric measurements of these gases when vented out of the ocean surface. The values also match the findings reported by Lueker et al. (2003) derived from atmospheric observations. Because of all these features linked together we can conclude that the model, although simplified, could give us results considered fairly robust for the purpose of our study.

3.4 *Thermal fluxes*

We now compare the seasonal cycle of the thermal component of the air–sea O_2 fluxes in the model with the following two alternate schemes: (1) the formula proposed by Keeling and Shertz (1992) and (2) the alternative method proposed by Jin et al. (2007). The Keeling and Shertz (1992) method is based on the following mathematical formulation:

$$\text{Flux} = \frac{\partial S}{\partial T}\,\frac{Q}{C_p \cdot \rho} \tag{23}$$

where $\frac{\partial S}{\partial T}$ is the partial derivative of gas solubility as function of temperature (T), Q is the ocean heat flux (W m^{-2}), C_p is the ocean heat capacity (3993 J Kg^{-1} $^{\circ}C^{-1}$) and ρ is the mean seawater density (1024.5 Kg m^{-3}, average ocean value). The Jin et al. (2007) method is a slight modification of the Keeling and Shertz (1992) formula:

$$\text{Flux} = \frac{1}{1.3} \cdot \frac{\partial S}{\partial T}\,\frac{Q}{C_p \cdot \rho} \cdot (t - 0.5 \cdot \text{month}) \tag{24}$$

where t is time expressed in months. Fig. 10 shows results for the thermal component of O_2 fluxes, zonally averaged. Results for Ar and N_2 (not shown) look very similar. The results show that the thermal components predicted by the model are phase lagged and reduced in amplitude compared to the predictions of the Keeling and Shertz (1992) formula, qualitatively consistent with Jin et al. (2007). However, some differences between the model and Jin et al. (2007) formula results are also evident. To help quantify

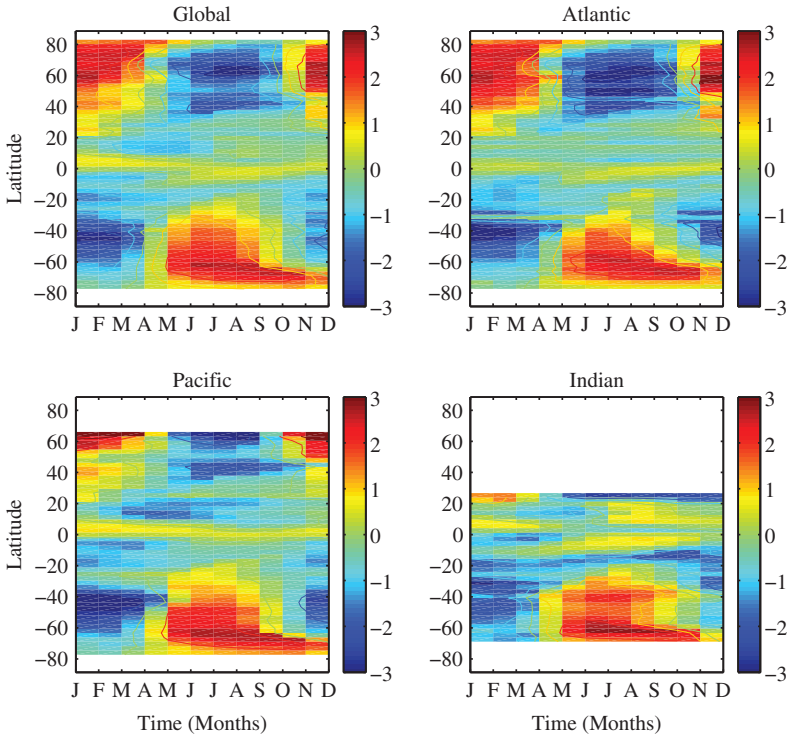

Fig. 8. Time/latitude plot of the natural logarithm of the ratio between the ventilation and production components of the air–sea O_2 fluxes for the global ocean (top left), Atlantic (top right), Pacific (bottom left) and Indian oceans (bottom right). Values are unit less and zonally averaged for each basin. Colour bar is in natural logarithmic scale.

the relationship between heat and thermal gas fluxes in our model, we extract the fundamental component (in a Fourier sense) of the seasonal cycle, which dominates the cycle. We compute this component by fitting a sine wave of a 1-yr period to the data, optimising both amplitude and phase (see Appendix A). Table 2 presents the results, based on fluxes averaged over 10° latitude bands. Polewards of 30° latitude, the amplitude ratios are typically around 0.93 in the Northern Hemisphere and range from 0.77 to 0.91 in the Southern Hemisphere. Except at high southern latitudes, we find smaller amplitude reductions compared to the ratio of $1/1.3 = 0.77$ indicated by the Jin et al. (2007) formula. The phase lags are in the range of 12–16 d, very similar to the 0.5 month estimate from Jin et al. (2007).

As discussed by Dietze and Oschlies (2005), the attenuation of the cycles compared to the prediction of the Keeling and Shertz (1992) formula arises due to three separate effects: (1) the finite mixed layer equilibration rates with the atmosphere which allows surface waters to be supersaturated or undersaturated; (2) water-mass mixing, which produce supersaturation due to the non-linearity of the solubility–temperature relation; and (3) the penetration of solar radiation below the mixed layer, which causes heating of subsurface waters which are out of contact with the atmosphere. While the first two effects are included in our model, the third is neglected, as our model assumes all solar radiation is absorbed in the surface layer. Dietze and Oschlies (2005) have shown that the solar effect, by itself, can account for a reduction in the amplitude of the seasonal O_2 flux by roughly 10% compared to what is expected from the Keeling and Shertz (1992) formula. If we adjust our amplitude ratios downward by multiplying by 0.9 to account for this neglected effect, the agreement with Jin et al. (2007) is reasonable. Nevertheless, it is clear that there are likely significant differences of order 10% between latitude bands that are not accounted for by the Jin et al. (2007) formula. The similarity in the phasing found by our model and that of Jin et al. (2007) suggests that the neglected solar effect has little influence on the phasing. Equatorward of 30° latitude, we find that the model in the tropics is likely to be influenced by complicated effects of mixing and possible model defects in tropical regions (Dietze and Oschlies, 2005). The Jin et al. (2007) formula may not be appropriate at low latitudes.

3.5. *Scaling considerations*

Equation (23) has also been used to scale between the thermally induced flux of one gas and another (Nevison et al., 2005). In this study, we test this scaling relationship

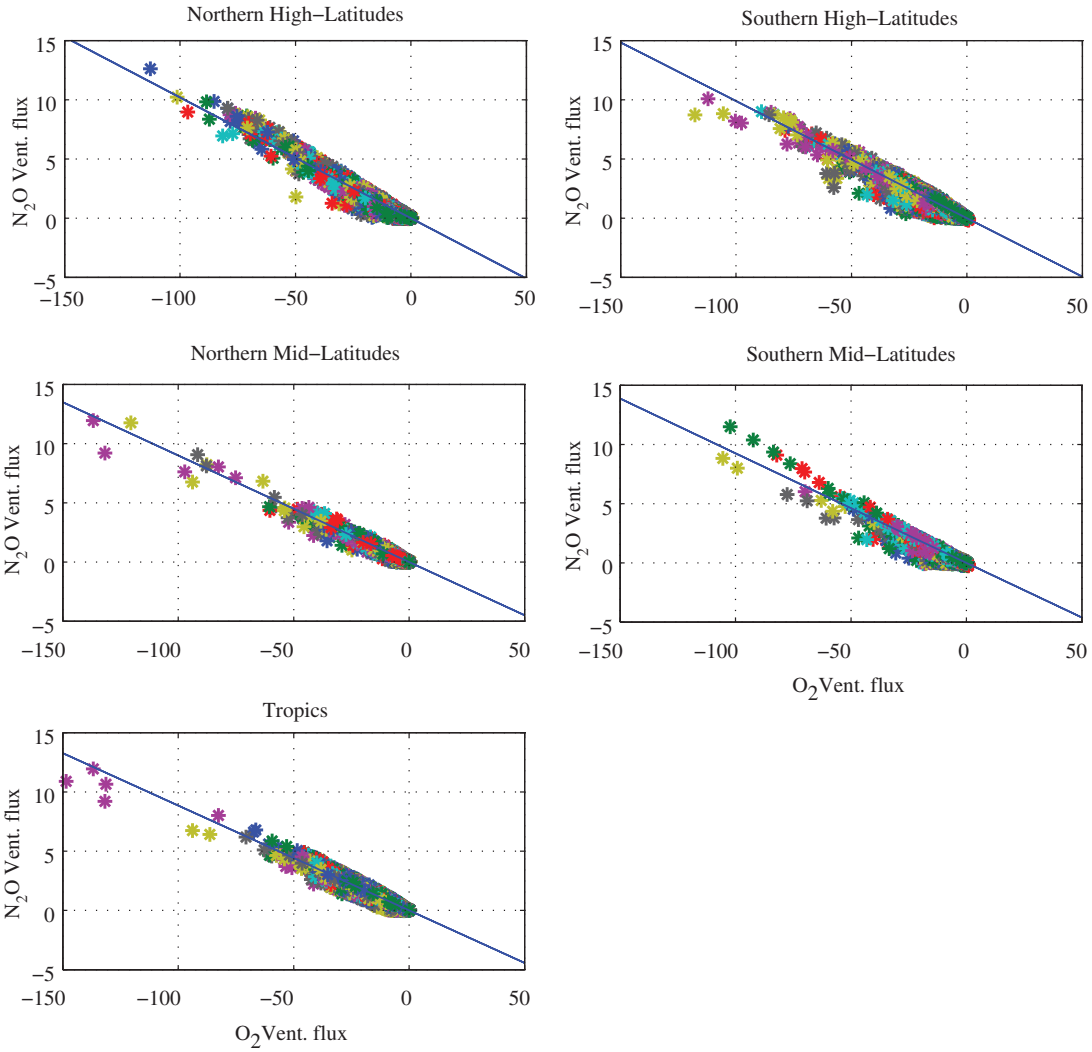

Fig. 9. Scatter plot of components of air–sea fluxes of O_2 and N_2O due to ocean ventilation in different latitudinal sectors of the global ocean. Units are mol m^{-2} yr^{-1} and mmol m^{-2} yr^{-1} for O_2 and N_2O fluxes, respectively. The blue line represents gas–gas relationship according to each slope value calculated using a least-square fit. Positive values indicate outgassing.

based on heat fluxes by comparing the flux ratios computed diagnostically from our OGCM with flux ratios computed from the equation proposed by Keeling and Shertz (1992). For example, for Ar and N_2, the use of Eq. (23) implies that this relationship can then be re-arranged, solving for F_{N_2}, as follows:

$$F_{N_2} = \frac{\left(\frac{\partial S}{\partial T}\right)_{N_2}}{\left(\frac{\partial S}{\partial T}\right)_{Ar}} \cdot F_{Ar} \tag{25}$$

The flux of N_2 could be thus estimated by computing the air–sea flux of Ar and provide the values of $\frac{\partial S}{\partial T}$ for both gases.

Here, we test Eq. (25) in the context of the OGCM. We compute the solubility factors for N_2 and Ar using the sea surface temperature and salinity computed by our OGCM. We then compute both the slope of the modelled air–sea fluxes of N_2 and Ar computed by our OGCM and the equivalent to this quantity based on the solubility ratios. The comparison shows that two values almost perfectly match (Table 3) suggesting that the relationship linking the air–sea fluxes of N_2 and Ar corresponds to the ratio of the solubility factors of both gases, confirming the theoretical framework shown above. We have compared similar ratios for the thermal component of the O_2 air–sea flux with the N_2 and Ar fluxes (see Appendix B for further details), as shown in (Table 3), and also found very good agreement with the scaling implied by Eq. (25). This shows that the errors incurred when applying the Keeling and Shertz (1992) approximation largely cancel out when applied to the ratio of the gas fluxes, as in Eq. (25).

Table 1. List of ratios of ventilation fluxes of O_2 and N_2O for five selected latitudinal bands where a zonal average is applied

Region	$F(^{Vent}_{N_2O})/F(^{Vent}_{O_2})$
$>30°$N	0.11 (0.02)
10°–30°N	0.09 (0.005)
10°N–10°S	0.09 (0.004)
10°–30°S	0.10 (0.008)
$>30°$S	0.11 (0.01)

We report the maximum values that correspond to the phase of ventilation between ocean surface and subsurface. Standard deviation is indicated in parenthesis and units are mmol/mol.

3.6. *Relationship between total O_2 and heat fluxes*

Table 2 also presents results for the relationship between the total O_2 flux (including also biological components) and the thermal flux expected from the Keeling and Shertz (1992) formula. This comparison is of interest in the context of Garcia and Keeling (2001) air–sea O_2 flux climatology. To interpolate the relatively sparse dataset for dissolved O_2, Garcia and Keeling (2001) invoked an empirical correlation between the total O_2 flux and the net air–sea heat flux, scaling the climatological heat flux to produce the O_2 flux fields. The approach implicitly assumes that net heat flux and O_2 flux are exactly in phase seasonally. In fact, the results in Table 2 show that, for latitudes poleward of 30° in both hemispheres, the total O_2 flux lags the Keeling and Shertz (1992) thermal flux by an average of $\sim$17 d (range of 13–21 d). Since the Keeling and Shertz (1992) formula is synchronised to the heat flux, the comparison also applies to the relationship between total O_2 flux and heat flux. Thus, our model results suggest that, for latitudes polewards of 30° of both hemispheres, the Garcia and Keeling (2001) climatology is likely to have a phasing error with the fluxes being too early by $\sim$17 d.

However, the general relationship between O_2 fluxes and heat fluxes breaks down in the tropical bands (between 10°N and 10°S), owing to the complex role played by upwelling (Keeling and Garcia, 2002). Also, a large fraction of the variability in the tropics is associated with frequencies other than the annual cycle. Therefore, our method, which focuses on the annual cycle, is not suitable for highlighting the dominant relationships in these bands.

4. Conclusions

We have used a physical–biogeochemical model of the global ocean where we explicitly represented the cycles of O_2, N_2O, Ar and N_2 and computed their respective air–sea fluxes that are driven by both physical and biogeochemical processes. We decomposed the air–sea O_2 flux into separate components driven by solubility changes, NCP and ventilation. Our results helped to evaluate a commonly used approach used to estimate summer-time NCP in which the fluxes driven by ventilation that are assumed to be negligible.

We estimated that this approximation is generally valid poleward of 30°N where the mismatch between fluxes based on heat fluxes and those directly computed by our model shows a difference between 20% and 30% for both hemispheres. In fact, our model results suggest that, in the northern high-latitude oceans in the period from June until August, the ventilation component of the air–sea O_2 flux is at a minimum and that the total flux is dominated by a combination of the thermal and NCP flux components. The same is affirmed for the southern high-latitude oceans in the period from December until February according to our model results. A potential caveat is that the global OGCM used for this study has a coarse vertical resolution (the thickness of the first two boxes is 50 and 70 m, respectively) that limits the model's ability to simulate fine scale upper ocean processes influencing primary production.

We have also shown that the ventilation component of the air–sea O_2 flux is strongly anti-correlated with the ventilation component of the N_2O flux, consistent with previous studies (Lueker et al., 2003; Nevison et al., 2005). Our model results show that the correction of solubility-driven fluxes proposed by Jin et al. (2007) can improve the match between prognostic (model generated) and diagnostic (based on heat fluxes) estimates, albeit more effectively in high-latitudes than in mid-latitude regions. We think that such a correction could be model dependent, although our investigation did not provide a final conclusion on this subject. Further investigation is needed by an ocean model with a more complete mixed layer scheme. A finer vertical resolution is also needed given the model we used did not implement these features and those factors could potentially impact the seasonal cycle of the air–sea gas fluxes.

Finally, we show that thermally driven fluxes of different gases are very strongly correlated with a ratio dictated by the solubility temperature dependencies. This supports the use of Ar/N_2 data for computing the thermal components of different gases in the atmosphere. It suggests that it may be sufficient in models to carry a single noble gas, such as Ar, as the fluxes of Ar can be used as a proxy for the thermal fluxes of other gases studied here (N_2 and O_2).

The model assumes a direct relationship between O_2 utilisation and N_2O production in the subsurface ocean. Some studies based on oceanic data (Emerson et al., 2004) and corroborated by the use of numerical models (Deutsch et al., 2005) suggest that the AOU in the interior of the North Pacific Ocean has increased in the last decades due to changes in ocean ventilation. This would imply a potential increase in N_2O production. Recently, it has been

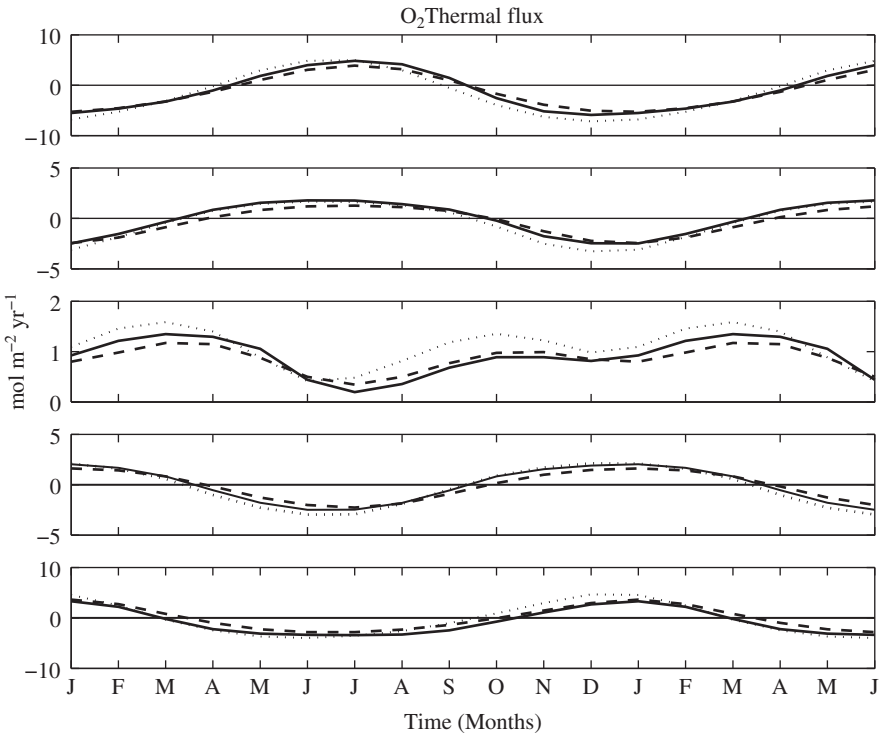

Fig. 10. Zonal average of the seasonal cycle of air–sea thermal O_2 flux of, from top to bottom, northern high-latitudes ($>30°$N); northern mid-latitudes (10–30°N); tropics (10°N–10°S); southern mid-latitudes (10–30°S); and southern high-latitudes ($>30°$S). The full line indicates the flux prognostically computed by the OGCM, the dotted line indicates the flux computed using the diagnostic formula of Keeling and Shertz (1992) based on ocean heat-fluxes and the dashed line indicates the air–sea flux calculated with both delaying and reduction factors according Jin et al. (2007). The first 6 months are repeated to show one and a half seasonal cycles. Positive values indicate outgassing.

Table 2. List of ratios of flux amplitude and (in parenthesis) difference in time lag corresponding to the seasonal peak and for each latitudinal band (first column)

Region	$F^{\mathrm{OGCM}}_{(\mathrm{Th})}/F^{\mathrm{KS92}}_{(\mathrm{Th})}$	$F^{\mathrm{OGCM}}_{(\mathrm{Tot})}/F^{\mathrm{KS92}}_{(\mathrm{Th})}$
60°–50°N	0.91 (12)	2.44 (21)
50°–40°N	0.92 (15)	2.5 (23)
40°–30°N	0.95 (16)	2.14 (14)
30°–20°N	1.18 (−2)	1.13 (3)
20°–10°N	0.85 (−4)	1.56 (−40)
10°–0°N	1.96 (−56)	11.5 (30)
10°–0°S	0.80 (11)	4.82 (32)
20°–10°S	0.86 (4)	1.48 (−6)
30°–20°S	0.91 (5)	1.58 (1)
40°–30°S	0.91 (13.38)	2.74 (15)
50°–40°S	0.86 (12)	3.43 (18)
60°–50°S	0.77 (12)	2.65 (13)

The second column gives values of the ratio of the thermal fluxes of O_2 from the OGCM over that computed according to Keeling and Shertz (1992) using the modelled net heat flux while in the third column we used the total O_2 computed by the OGCM instead of the thermal flux. Calculations are based on fits to global zonally averaged fluxes over indicated latitude bands. Ratios have no units and lags are indicated in days.

suggested that in the last decades the westerly winds over the Southern Ocean have increased their strength with negative consequences for the uptake of anthropogenic CO_2 uptake (Le Quéré et al., 2007). This increase in wind speed could potentially enhance the upwelling in the Southern Ocean and the outgassing of N_2O as a potential feedback effect of climate change because of its greenhouse effect.

Ocean biogeochemical models, such as the one set up for this study (with separated tracers to isolate specific processes) embedded in state-of-the-art OCGMs and

Table 3. Scaling factors between air–sea gas fluxes calculated by (left) heat-flux formulas and by (right) the use of the ocean general circulation model (OGCM) used for this study

Gas–gas relationship	S-ratio	OGCM
$F_{\mathrm{N_2}} = f(F_{\mathrm{Ar}})$	34	34.5 (0.9)
$F_{\mathrm{O_2(Th)}} = f(F_{\mathrm{Ar}})$	20.82	20.76 (0.9)
$F_{\mathrm{O_2(Th)}} = f\left(F_{\mathrm{N_2}}\right)$	0.61	0.6 (0.9)

Values in parenthesis indicate the correlation coefficients calculated for the OGCM output.

forced by climate variability can potentially help to diagnose whether the fluxes of N_2O will directly follow the expected increasing trends in key areas, such as the North Pacific Ocean or the Southern Ocean. Furthermore, a progressive global trend of ocean warming would imply a process of ocean de-oxygenation (Keeling et al., 2010) that would certainly alter the biogeochemical dynamics in the ocean interior with potential consequences for N_2O production and its outgassing to the lower atmosphere, with a potential impact on the radiative forcing of the Earth's atmosphere.

5. Acknowledgements

We sincerely thank Stephanie Dutkiewicz for making the biogeochemical code available, Parv Suntharalingam for her useful guidance when implementing the N_2O cycle into our model, Lynne Merchant for editing figures, Stephen Walker for helping with the computation of harmonics of heat-based air–sea gas fluxes and two anonymous reviewers who contributed with their comments to greatly improve the quality of the manuscript. MM and CDN were financially supported by the NASA Ocean Biology and Biogeochemistry Program through the grant NNX08AB48G. MM also acknowledges financial support from the Postdoctoral Program fellowship at Scripps Institution of Oceanography. We also thank Dimitris Menemenlis and the ECCO-Phase 2 project for making the computing facilities at the NASA Advanced Supercomputing Division accessible to us. This work was created using the Tellus LATEX2ε class file.

Appendix A

We performed a harmonic fit to the seasonal fluxes of thermally driven air–sea O_2 fluxes calculated with three methods using the least square fit method based on a linear system of equations. The coefficients derived from the harmonic fit to calculate both the amplitude and the time lag of the seasonal peak are computed to match the following function:

$$\text{Flux} = A' \cdot \cos(2\pi(t - t_{\max})) \tag{26}$$

where A' is the amplitude of the flux and $t_{\max}$ is the time of seasonal peak over a period of 1 yr, The O_2 fluxes calculated according to Keeling and Shertz (1992) and Jin et al. (2007) have been masked using the same sea–ice cover imposed to the OGCM to compare them to those computed by the ocean biogeochemical model.

Appendix B

We calculated the thermally driven fluxes of O_2 as function of both Ar and N_2 fluxes adopting the scaling theory explained in the text, as follows:

$$F_{O_2(\text{Th})} = \frac{\left(\frac{\partial S}{\partial T}\right)_{O_2}}{\left(\frac{\partial S}{\partial T}\right)_{Ar}} \cdot F_{Ar} \tag{27}$$

$$F_{O_2(\text{Th})} = \frac{\left(\frac{\partial S}{\partial T}\right)_{O_2}}{\left(\frac{\partial S}{\partial T}\right)_{N_2}} \cdot F_{N_2} \tag{28}$$

Units of gas fluxes are in mol m^{-2} s^{-1}.

References

Bates, N. R., Best, M. H. and Hansell, D. A. 2005. Spatio-temporal distribution of dissolved inorganic carbon and net community production in the Chukchi and Beaufort Seas. *Deep Sea Res-II*. **52**(24–26), 3303–3323.

Beman, J. M., Chow, C.-E., King, A. L., Feng, Y., Fuhrman, J. A. and co-authors. 2011. Global declines in ocean nitrification rates a consequence of ocean acidification. *Proc. Natl. Acad. Sci*. **108**, 208–213.

Bennington, V., McKinley, G. A., Dutkiewicz, S. and Ullman, D. 2009. What does chlorophyll tell us about export and air–sea CO_2 flux variability in the North Atlantic? *Global Biogeochem. Cycles*. **23**, GB3002. DOI: 10.1029/2008GB003241.

Bopp, L., Le Quéré, C., Heimann, M., Manning, A. C. and Monfray, P. 2002. Climate-induced oceanic oxygen fluxes: implications for the contemporary carbon budget. *Global Biogeochem. Cycles*. **16**, 2. DOI: 10.1029/2001GB001445.

Brix, H., Gruber, N., Karl, D. M. and Bates, N. R. 2006. On the relationships between primary, net community, and export production in subtropical gyres. *Deep-Sea Res–II*. **579**(5–7), 698–717.

Butler, J. H., Elkins, J. W. and Thompson, T. M. 1989. Tropospheric and dissolved N_2O of the west Pacific and east Indian Oceans during El Nino Southern Oscillation event of the 1987. *J. Geophys. Res*. **94**, 14865–14877.

Craig, H. and Hayward, T. 1987. Oxygen supersaturation in the ocean—biological versus physical contributions. *Science*. **235**(4785), 199–202.

Deutsch, C., Emerson, S. and Thompson, L. 2005. Fingerprints of climate change in North Pacific oxygen. *Geophys. Res. Lett*. **32**, L16604. DOI: 10.1029/2005GL023190.

Dietze, H. and Oschlies, A. 2005. On the correlation between air–sea heat flux and abiotically induced oxygen gas exchange in a circulation model of the North Atlantic. *J. Geophys. Res. – Oceans*. **110**, C09016. DOI: 10.1029/2004JC002453.

Dore, J. E., Popp, B. N., Karl, D. M. and Sansone, F. J. 1998. A large source of atmospheric nitrous oxide from subtropical North Pacific surface waters. *Nature*. **396**, 63–66.

Dutkiewicz, S., Follows, M. J. and Parekh, P. 2005. Interactions of the iron and phosphorus cycles: a three-dimensional study. *Global Biogeochem. Cycles*. **19**, GB1021. DOI: 10.1029/2004GB002342.

Emerson, S., Watanabe, Y. W., Ono, T. and Mecking, S. 2004. Temporal trends in apparent oxygen utilization in the upper pycnocline of the North Pacific: 1980–2000. *J. Oceanogr.* **60**, 139–147.

Garcia, H. G. and Gordon, L. I. 1992. Oxygen solubility in seawater: better fitting equations. *Limnol. Oceanogr.* **37**, 1307–1312.

Garcia, H. G. and Keeling, R. F. 2001. On the global oxygen anomaly and air–sea flux. *J. Geophys. Res. – Oceans.* **106**, 31155–31166.

Gent, P. R. and McWilliams, J. C. 1990. Isopycnal mixing in the ocean circulation models. *J. Phys. Oceanogr.* **20**, 150–155.

Hamme, R. and Emerson, S. 2004. The solubility of neon, nitrogen, and argon in distilled and seawater. *Deep-Sea Res. I.* **51**(11), 1517–1528.

Hendricks, M. B., Bender, M. L. and Barnett, B. A. 2004. Net and gross O_2 production in the southern ocean from measurements of biological O_2 saturation and its triple isotope composition. *Deep-Sea Res. I.* **51**, 1541–1561.

Horrigan, S. G., Carlucci, A. F. and Williams, P. M. 1981. Light inhibition of nitrification in sea-surface films. *J. Mar. Res.* **39**, 557–565.

Ito, T., Parekh, P., Dutkiewicz, S. and Follows, M. J. 2005. The antarctic circumpolar productivity belt. *Geophys. Res. Lett.* **32**, L13604. DOI: 10.1029/2005GL023021.

Jian, S., Stone, P. H. and Malanotte-Rizzoli, P. 1999. An assessment of the geophysical fluid dynamics laboratory ocean model with coarse resolution: annual-mean climatology. *J Geophys Res.* **104**, 25623–25645.

Jin, X., Najjar, R. G., Louanchi, F. and Doney, S. C. 2007. A modeling study of the seasonal oxygen budget of the global ocean. *J. Geophys. Res. – Oceans.* **112**, C05017. DOI: 10.1029/2006JC003731.

Keeling, R. F. and Garcia, H. E. 2002. The change in oceanic O_2 inventory associated with recent global warming. *Proc. US Natl. Acad. Sci.* **99**(12), 7848–7853.

Keeling, R. F., Koertzinger, A. and Gruber, N. 2010. Ocean Deoxygenation in a Warming World. *Annl. Rev. Mar. Sci.* **2**, 199–229.

Keeling, R. F., Najjar, R. P., Bender, M. L. and Tans, P. P. 1993. What atmospheric oxygen measurements can tell us about the global carbon cycle. *Global Biogeochem. Cycles.* **7**(1), 37–67.

Keeling, R. F. and Shertz, S. R. 1992. Seasonal and interannual variations in atmospheric oxygen and implications for the global carbon cycle. *Nature.* **358**, 723–727.

Law, C. S. and Owens, N. J. P. 1990. Significant flux of atmospheric nitrous oxide from the northwest Indian Ocean. *Nature.* **346**, 826–828.

Le Quéré, C., Rödenbeck, C., Buitenhuis, E. T., Conway, T. J., Lagenfelds, R. and co-authors. 2007. Saturation of the Southern Ocean CO_2 sink due to recent climate change. *Science.* **319**(5863), 570. DOI: 10.1126/science.1147315.

Lueker, T. J., Walker, S. J., Vollmer, M., Keeling, R. F., Nevison, C. D. and co-authors. 2003. Coastal upwelling air–sea fluxes revealed in atmospheric observations of O_2/N_2, CO_2 and N_2O. *Geophys. Res. Lett.* **30**, 1292. DOI: 10.1029/2002GL016615.

Marshall, J., Hill, C., Perelman, L. and Adcroft, A. 1997. Hydrostatic, quasi-hydrostatic and nonhydrostatic ocean modeling. *J. Geophys. Res.* **102**(C3), 5733–5752.

Matear, R. J. and Hirst, A. C. 2003. Long-term changes in dissolved oxygen concentrations in the ocean caused by protracted global warming. *Global Biogeochem. Cycles.* **17**(4), 1125. DOI: 10.1029/2002GB001997.

Najjar, R. G. and Keeling, R. F. 1997. Analysis of the mean annual cycle of the dissolved oxygen anomaly in the World Ocean. *J. Mar. Res.* **55**, 117–151.

Najjar, R. G. and Keeling, R. F. 2000. Mean annual cycle of the air–sea oxygen flux: a global view. *Global Biogeochem. Cycles.* **14**(2), 573–584.

Naqvi, S. W. A., Bange, H. W., Farías, L., Monteiro, P. M. S., Scranton, M. I. and co-authors. 2009. Coastal hypoxia/anoxia as a source of CH4 and N_2O. *Biogeosci. Discuss.* **6**(5), 9455–9523.

Naqvi, S. W. A., Yoshinari, T., Jaykumar, D. A., Altabet, M. A., Narvekar, P. V. and co-authors. 1998. Budgetary and biogeochemical implications of N_2O isotope signatures in the Arabian Sea. *Nature.* **384**, 462–464.

Nevison, C. D., Butler, J. H. and Elkins, J. W. 2003. Global distribution of N_2O and D N_2O-AOU yield in the subsurface ocean. *Global Biogeochem Cycles.* **17**, 1119. DOI: 10.1029/2003GB002068.

Nevison, C. D., Keeling, R. F., Kahru, M., Manizza, M., Mitchell, B. G. and co-authors. 2012. Estimating net community production of the Southern Ocean based on atmospheric potential oxygen and satellite ocean color data. *Global Biogeochem Cycles.* **26**, 1. DOI: 10.1029/2011GB004040.

Nevison, C. D., Keeling, R. F., Weiss, R. F., Popp, B. N., Jin, X. and co-authors. 2005. Southern Ocean ventilation inferred from seasonal cycles of atmospheric N_2O and O_2/N_2 at Cape Grim, Tasmania. *Tellus-B.* **57**, 218–229.

Nevison, C. D., Weiss, R. F. and III, D. J. E. 1995. Global oceanic emissions of nitrous oxide. *J Geophys Res.* **100**, 15809–15820.

Riser, S. R. and Johnson, K. S. 2008. Net production of oxygen in the subtropical ocean. *Nature.* **451**(7176), 323–325. DOI: 10.1038/nature06441.

Schlitzer, R. 2000. Applying the adjoint method for global biogeochemical modeling. In: *Inverse Methods in Global Biogeochemical Cycles.* (eds. P. Kasibhatla, M. Heimann, D. Hartley, N. Mahowald, R. Prinn and P. Rayner) Vol. 114, AGU Geophys. Monograph Series, pp. 107–124.

Shaffer, G., Olsen, S. M. and Pedersen, J. O. 2009. Long-term ocean oxygen depletion in response to carbon dioxide emissions from fossil fuels. *Nat. Geosci.* **2**, 105–109.

Shulenberger, E. and Reid, J. 1981. The Pacific shallow oxygen maximum, deep chlorophyll maximum, and primary production, reconsidered. *Deep-Sea Res.* **28**, 901–919.

Stanley, R. H. R., Kirkpatrick, J. B., Cassar, N., Barnett, B. A. and Bender, M. L. 2010. Net community production and gross primary production rates in the western equatorial Pacific. *Global Biogeochem. Cycles.* **24**, GB4001. DOI: 10.1029/2009GB00365.

Suntharalingam, P., Buitenhuis, E., Le Quéré, C., Dentener, F., Nevison, C., Butler, J. H., Bange, H. W.,and Forster, G. 2012. Quantifying the impact of anthropogenic nitrogen deposition on oceanic nitrous oxide. *Geophys. Res. Lett.* **39**, L07605. DOI: 10.1029/2011GL050778.

Suntharalingam, P. and Sarmiento, J. L. 2000. Factors governing the oceanic nitrous oxide distribution: simulations with an ocean general circulation model. *Global Biogeochem. Cycles.* **14**(1), 429–454.

Suntharalingam, P., Sarmiento, J. L. and Toggweiler, J. R. 2000. Global significance of nitrous-oxide production and transport from oceanic low-oxygen zones: a modeling study. *Global Biogeochem. Cycles.* **14**(4), 1353–1370.

Trenberth, K., Olson, J. and Large, W. 1989. A global wind stress climatology based on EMCWF analysis. *Technical report*. Boulder, CO, NCAR.

Walter, S., Bange, H. W., Breitenbach, U. and Wallace, D. W. R. 2006. Nitrous oxide in the Atlantic Ocean. *Biogeosciences.* **3**, 607–619.

Wanninkhof, R. 1992. Relationship between wind speed and gas exchange over the ocean. *J. Geophys. Res.* **97**, 7373–7382.

Warren, B. A. 1983. Why is no deep water formed in the North Pacific? *J. Mar. Res.* **41**, 327–347.

Weaver, A. J., Bitz, C. M., Fanning, A. F. and Holland, M. M. 1999. Thermohaline circulation: high-latitude phenomena and the difference between the Pacific and the Atlantic. *Ann. Rev. Earth Planet. Sci.* **27**, 231–285.

Weiss, R. F. and Price, B. A. 1980. Nitrous oxide solubility in water and seawater. *Mar. Chem.* **8**, 347–359.

Yoshinari, T. 1976. Nitrous oxide in the sea. *Mar. Chem.* **4**, 189–202.